Solid Electrolyte Interphase (SEI) Formation on the Graphite Anode in Electrolytes Containing the Anion Receptor Tris(hexafluoroisopropyl)borate (THFIPB)

Ahmet Oguz Tezel[1,2], Daniel Klaus Streich[2], Aurélie Guéguen[2], Maria Hahlin[3], Svein Sunde[1], Kristina Edström[3], Petr Novák[2], Ann Mari Svensson[1]

[1] Norwegian University of Science and Technology, Department of Materials Science and Engineering, N-7491 Trondheim, Norway

[2] Paul Scherrer Institute, Electrochemistry Laboratory, CH-5232 Villigen PSI, Switzerland

[3] Uppsala University, Department of Physics and Astronomy, Box 516, SE-751 20 Uppsala, Sweden

ABSTRACT

Addition of small amounts of tris(hexafluoroisopropyl)borate (THFIPB) has previously been shown to improve the capacity of graphite anodes in a wide temperature window during long-term cycling in electrolytes based on $LiPF_6$ in ethylene carbonate (EC) and diethylene carbonate (DMC) solvents. Here, we demonstrate that the addition of THFIPB accelerates the $LiPF_6$ hydrolysis, and consumes residual water. The SEI formation and composition was studied by operando electrochemical mass spectrometry (OEMS), X-ray photoelectron spectroscopy (XPS), and ex-situ diffuse reflectance spectroscopy (DRIFT). Differences in the surface products are observed for the THFIPB containing electrolyte already upon exposure of graphite anodes to the electrolyte. Both the mechanism and the kinetics of the EC reduction reaction are affected, as evidenced by the shift in the C_2H_4 evolution peak to higher potentials as compared to the reference electrolyte. Addition of THFIPB leads to formation of a SEI layer enriched in inorganic components; salt reduction products at high potentials, and inorganic carbonate at lower potentials. The SEI formed is more conductive but slightly less passivating. The SEI formed in the reference electrolyte is dominated by organic compounds, also at high potentials, facilitated by the trace amounts of water inevitably found in the electrolyte.

INTRODUCTION

Graphite is the dominating anode material for Li-ion batteries, and the formation of a passivation layer on the surface, the solid electrolyte interphase (SEI), is critical for the performance. For the commonly employed electrolyte consisting of $LiPF_6$ salt in an EC containing electrolyte it is generally agreed that the solvent reduction products lithium ethylene dicarbonate (LEDC), $ROCO_2Li$, ROLi, as well as salt and impurity reduction products including Li_xPF_y, $Li_xPF_yO_z$, LiF, Li_2O, and Li_2CO_3 are among the main constituents of the SEI [1, 2, 3]. The structure of the SEI is generally believed to be both "mosaic", as well as a bilayer structure with inner, inorganic components, and an outer, organic, layer. The inner layer is typically composed of LiOH, Li_2O and LiF [4, 5]. Li_2CO_3 might be an exception, as it seems to be more uniformly distributed in the SEI [6]. The presence of Li_2CO_3 could also result from exposure to moisture during the sample handling [7]. It is highly likely that the transport of Li^+ is facilitated by the grain boundaries in the mosaic structure [8, 9].

Trace amounts of water are inevitably found in industrial quality battery electrolytes (of the order of tens of ppm). $LiPF_6$, the salt used in almost all commercial Li-ion battery cells, is known to decompose to PF_5, which again reacts with water to form POF_3 and HF [10, 11]:

$$PF_5 + H_2O \rightarrow POF_3 + 2HF \qquad \text{(eq. 1)}$$

The presence of water and PF_5/POF_3/HF in electrolytes does also affect the SEI formation. Water will reduce on the surface to form LiOH or Li_2O [12], in combination with evolution of H_2 (g) [12, 13, 14]. Furthermore, water will react with organic SEI compounds, like $ROCO_2Li$ to form Li_2CO_3, CO_2, and glycol [13, 15]. PF_5 is known to catalyze the EC ring opening [16]. The evolution of hydrogen on battery graphite from HF containing carbonate electrolytes was demonstrated in Ref. [17], where HF was formed upon addition of H_2O in $LiPF_6$-carbonate electrolyte mixtures and subsequent ageing. Hydrogen evolution was observed from around 2 V vs. Li/Li^+, with a sharp increase in the current at around 0.5 V. The fact that the current was correlated to the concentration of HF was taken as an evidence for the electrochemical transformation of the HF impurity to LiF and H_2 [17].

The formation and quality of SEI layers can be tailored by careful selection of electrolyte additives. Examples of reductive and reaction type additives are fluoroethylene carbonate (FEC) [18, 19, 20, 21] and vinylene carbonate [22, 23, 24], whose primary aim is to form a

stable SEI by sacrificially reducing above the solvent reduction potentials. FEC and VC are now commonly used additives due to the positive impact on the formation of the kinetically stable SEI. Another class of additives are the so-called anion receptors (AR), originally proposed to modify the electrolyte properties [25, 26]. The effect of anion receptors on NMC cathodes, graphite anodes, as well as full cells has been investigated in several works [27, 28, 29, 30]. Positive effects on performance of electrodes or cells upon addition of anion receptors have been reported, like the addition of tris(pentafluorophenyl)borane TPFPB [26, 27, 28] or tris(hexafluoroisopropyl)borate (THFIPB) [30], provided that the concentration is optimized. Addition of TPFPB to a carbonate electrolyte with $LiPF_6$ was found to accelerate the decomposition of $LiPF_6$ to release PF_5 [31]. As THFIPB is a strong Lewis acid, as evident from its ability to facilitate LiF dissolution in carbonate solvents [32], it is also expected to accelerate the decomposition. PF_5, also a strong acid, may then further react with the trace water unavoidably present in the electrolyte and cell components, to ultimately yield POF_3 (which is a Lewis acid too) and HF according to eq. 1. This finding agrees well with the reports on fluoride affinities of various anion receptors [33].

We have shown in a previous study that graphite electrodes experienced a lower capacity fade over 200 cycles in a 1M $LiPF_6$ in 1:1 EC:DMC (LP30) electrolyte with small additions of THFIPB compared to the electrolyte without the additive [34]. Significant differences in the morphology of the SEI layers obtained in the two electrolytes could be verified by SEM. The results were suggested to be related to the accelerated decomposition of $LiPF_6$ and generation of PF_5 (as a result of THFIPB-F^- binding). Overall, the addition of THFIPB lead to formation of a more conductive, more stable, but slightly less passivating SEI. In full cells, the slightly lower coulombic efficiency in the first charge counteracted the benefits observed in half cells.

The aim of this work is to provide in-depth understanding of the SEI formation process on graphite in THFIPB containing electrolytes. We put forward the hypothesis that the observed differences in the SEI formation are related to the accelerated $LiPF_6$ decomposition in the presence of THFIPB, leading to an electrolyte with excess amounts of PF_5, POF_3, and HF (see eq. 1). A variety of electrochemical and spectroscopic techniques has been applied for the investigations. These include operando X-ray diffraction (XRD), OEMS before and during cycling, post-mortem DRIFTS analysis of the SEI layers, as well as XPS of the SEI layers during the SEI forming process. The effect of THFIPB on the bulk electrolyte was also

investigated by Fourier transformed infrared Spectroscopy (FTIR), in order to identify possible effects on solvation structure of the salt. In this manner, differences in the SEI formation and composition could be verified.

EXPERIMENTAL

Electrode preparation and electrochemical characterization. — All electrodes were prepared using a graphite active material, SLP30 (IMERYS Graphite & Carbon), polyvinylidene difluoride binder (Kynar® HSV 900), and Super P conductive filler (IMERYS Graphite & Carbon) with a weight ratio of 80:10:10, respectively, dispersed in N-methyl pyrrolidone (NMP; Sigma-Aldrich). The slurry was then coated onto a copper foil via doctor blade method. Li foil was used as a counter electrode which served as a reference electrode as well. A monolayer polypropylene separator (CELGARD 2400) was placed between the working and counter electrode. LP30 (1 M $LiPF_6$ in EC/DMC 1:1 weight ratio; BASF) was used as the reference electrolyte for all the experiments. THFIPB (TCI Europe, N.V.) was added at 0.025 (AR25) and 0.075 (AR75) molar concentrations, respectively. The cells were assembled in an argon-filled dry box with a water and oxygen level of <1 ppm. The water content was measured by Karl Fisher titration and confirmed to be below 20 ppm. Electrochemical measurements were performed using a computer controlled capture system (CCCC, Astrol Electronic AG). Galvanostatic lithiation/delithiation was conducted within a potential range of 0.005 - 1.5 V vs. Li/Li^+. All electrodes were cycled at 10 mA/g and 50 mA/g, respectively, during the first and second cycle. A potentiostatic step was included at the end of each cut-off potential, to ensure full lithiation/delithiation. For the first lithiation, this involved reducing the specific current to 5 mA/g, and for the subsequent cycles the step was applied until the specific current dropped to 10% of the initial value.

DRIFT— Electrodes were extracted from cells, rinsed with DMC, and dried in an argon environment overnight at room temperature, followed by a vacuum drying procedure of 2 hours to remove the residual electrolyte. The electrode coating was then scraped from the copper foil and diluted in 1:100 (wt.%) ratio with ground KBr powder. 1.5:150 mg ratio of sample/KBr was maintained for all the samples in order to allow comparison between the measurements. The mixture was then filled in a hermetically sealed accessory in a glove box environment for the measurement. For each spectrum, 512 scans were collected at 4 cm^{-1} resolution over the spectral range 4000-800 cm^{-1}. All the spectra were recorded using standard FTIR spectrometers (Perkin Elmer System 2000, Bruker Vertex 70v).

FTIR — Electrolyte mixtures were prepared in the glove box. The samples were stored in Teflon vials to avoid HF/SiO_2 interaction. All measurements were carried out with Perkin Elmer 2000 equipped with golden gate diamond ATR sample holder (Portmann Instruments AG). All spectra were recorded in attenuated total reflection (ATR) mode. All spectra were acquired at 4 cm^{-1} resolution with 10 scans collectedover the range 4000-400 cm^{-1}.

OEMS — The slurry for making the working electrodes was prepared as described above, and was then casted onto a monolayer polypropylene separator (CELGARD 2400) via doctor blade method. The MS setup has been described elsewhere [35]. 500 µL of electrolyte was used in the electrochemical cell. 0.7 mL of gas was extracted from the head space and replaced by pure argon gas. The extracted gas was then transferred to the inlet of the MS through argon flow. Such gas extraction occurred every 15 min during a linear potential scan at a rate of 25 µV/s.

HAXPES — The HAXPES measurements were performed at the KMC-1 beamline using the HIKE end station at the BESSY II synchrotron (Helmholtz Zentrum, Berlin, Germany). Excitation energies of 2005 eV and 6015 eV were applied, based on previous studies of SEI layers of graphite anodes [5]. The measurement time was kept as short as possible, while still discerning the shape of a spectrum, in order to avoid effects of radiation damage on the spectra. The electron take-off angle was 80^o defined relative to the surface plane of the sample, and the take-off direction was collinear with the e-vector of the incident photon beam. The spectra were energy calibrated using the C-H features of the graphite negative electrode set to 285 eV. After exposure to electrolyte for 24 hrs or cycling to a set potential, the electrodes were transferred to the analysis chamber in a specially designed transfer chamber to avoid exposure to air [36]. The samples were washed with DMC and dried prior to the investigation.

IN-SITU XRD — The in-situ XRD cell made of Ti and PEEK was assembled in a glove box. A thin Li-foil placed at the bottom of the cell was used as counter electrode. A glass-fiber separator was put on top of the Li-foil and 200 µL electrolyte were dropped on it. A self-standing working electrode was placed on the top of the separator. The self-standing electrode was prepared by mixing 70 wt % graphite (SLP30), 10 wt % Super P carbon black, and 20 wt % Kynarflex binder. The slurry was cast onto a Teflon foil via doctor blading and dried at 120 ^oC under vacuum overnight. The electrode sheet was then peeled off from the Teflon foil. After all cell components were in place, the top lid of the cell was screwed to

keep the cell components together. The top lid was covered by a window made of 100 µm thick Be disk. Finally, the pressure in the cell was slightly decreased to ensure that a rubber O-ring seals the cell properly. The XRD scans were recorded while the graphite was galvanostatically charged at 10 mA/g to 10 mV (vs. Li^+/Li). The measurement was performed at room temperature using Panalytical Empyrean diffractometer using Cu K-α radiation.

RESULTS and DISCUSSION

FTIR analysis of the electrolyte--- At first it was important to understand the effect of the anion receptor on the electrolyte structure. Therefore, FTIR spectra of the various electrolyte components were collected (Figure 1). We were able to identify some of the peaks that have not been clearly attributed to any species in the literature yet. The main purpose was to distinguish between Li-solvent and PF_6^--solvent absorptions; therefore, various lithium salts including $LiClO_4$ were employed for improved reliability of our assignments.

The first goal was to identify the PF_6^- signal in order to determine whether the anion is interacting with the THFIPB or not. To achieve this, we started by collecting the neat DMC and DMC+$LiPF_6$ spectra. In Figure 1, the absorption at 1751 cm^{-1} in neat DMC is due to the carbonyl (C=O) stretching vibration [37]. A band splitting occurs when $LiPF_6$ is dissolved in DMC; while the original band at 1751 cm^{-1} is preserved, a new band appears at 1720 cm^{-1}. This splitting was suggested to originate from the Li^+ solvation of the DMC molecules through carbonyl-Li^+ interaction [37]. In order to verify this assignment, 1M $LiClO_4$ was dissolved in DMC and the corresponding spectrum was recorded. It is seen that the same band splitting as in $LiPF_6$ electrolyte occurs in $LiClO_4$ electrolyte too. Thus, it is highly probable that the absorption at 1720 cm^{-1} is due to the Li^+ solvation of the DMC molecules, as both salts have only Li^+ in common.

Figure 2 shows the spectral region 900-700 cm^{-1} where isolated PF_6^- and ion-pairs absorb [37]. When $LiPF_6$ is dissolved in EC and DMC, strong absorptions at 839 and 842 cm^{-1} in EC and DMC, respectively, are observed, which are absent in neat EC and DMC spectra. This indicates that these bands result from the salt addition and originate from the PF_6^- since Li^+ (single ion) cannot have any feature in that FTIR spectral region. In addition to this, a broad shoulder appears at 867 cm^{-1} in DMC which is absent in EC electrolyte. It has been suggested that $Li^+\cdots PF_6^-$ ion pairs absorb at 867 cm^{-1} [37] with an associated reduction in the original PF_6^- band (842 cm^{-1}) intensity due to the ion pair formation. The presence of ion-pairs indicates incomplete dissociation of $LiPF_6$ in DMC due to the latter being a low dielectric

solvent. This band is seen to vanish when 1M $LiPF_6$ is dissolved in EC as the high dielectric constant of EC facilitates ion separation.

Similarly, the band at 741 cm^{-1} (ν_1 mode of PF_6^-) can be discussed and analyzed within this framework. It has been demonstrated that the ν_1 mode of isolated PF_6^- is only Raman active; however, when PF_6^- forms ion pairs with Li^+, the ν_1 mode of PF_6^- also becomes IR active [38]. This phenomenon at 741 cm^{-1} is obvious in Figure 2, wherein ν_1 band is seen in DMC and not in EC.

In order to examine the effect of the THFIPB on the electrolyte properties, FTIR difference spectra obtained by subtracting DMC+1 M $LiPF_6$ from DMC+1 M $LiPF_6$+THFIPB and EC+1 M $LiPF_6$ from EC+1 M $LiPF_6$+THFIPB are plotted in Figure 3. The negative-going peaks in the difference spectra indicate a decrease in the concentration of the corresponding species upon THFIPB addition. Isolated PF_6^- manifests itself at 840 cm^{-1} [37, 38]. The peak that appears at 867 cm^{-1} is due to the absorption of $Li^+\cdots PF_6^-$ ion pairs [37, 38]. Both difference spectra show significant negative peaks at 840 cm^{-1} suggesting that the isolated PF_6^- ions are affected by the presence of THFIPB. This is the most significant feature of the difference spectra. Less significant negative peaks are observed for the bands at 970 cm^{-1} for EC and at 790 cm^{-1} for DMC. Other bands of the carbonate solvents are overlapping. We may now propose, based on FTIR results showing the decrease in PF_6^- concentration in AR25 electrolyte, that the origin of the THFIPB-PF_6^- interaction may be the stronger F^- affinity of THFIPB than that of PF_5 resulting in the decomposition of the PF_6^- anion, as expressed in eq. 1.

It has been verified both theoretically (by DFT calculations) and experimentally (by electrospray ionization mass spectrometry, ESI-MS) that the dominating species in an 1M $LiPF_6$ EC:DMC electrolyte containing 0.1 wt % TPFPB is the complex [TPFPB + F^-] [39], in line with the findings here for a similar anion receptor.

The ratio of the peaks at 867 cm^{-1} and 840 cm^{-1}, as well as the ratio of the distorted band and the original band for the O-C-O stretching at 1268 cm^{-1} [40] and C=O stretching at 1751 cm^{-1} [40] showed similar values for the LP30 and AR25 electrolytes. As these ratios would depend on the presence of ion-pairs, the results imply that no significant difference in ion-pairing between LP30 and AR25 could be identified based on the FTIR spectra.

OEMS--- Mass spectrometry analysis (Figure 4) was carried out during the first linear sweep voltammetry (Figure 4 a), following a four hours rest time to identify gases evolving from both LP30 and AR25 electrolytes.

POF_3 evolution (or rather a mixture of POF_3 and PF_5, as discussed in Ref. [41]) is observed in AR25 once the charging starts and the potential drops below 2.9 V (Figure 4b). The POF_3 (PF_5) evolution is accompanied by H_2 evolution at 2.7 V (Figure 4c). In graphite/Li half cells, H_2 evolution is typically attributed to the reduction of residual water which is inevitably present in the electrolytes (around 20 ppm) [13, 42, 43]. In all these works, the amount of hydrogen evolved was found to be correlated to the amount of water in the electrolyte. However, water reduction starts at potentials lower than ca 1.9 V, and cannot be the origin of the peak at 2.7 V. We also exclude the possibility that water is reduced at the metallic Li counter electrode, as no H_2 peak is observed for the LP30 electrolyte at this potential. Evolution of H_2 from HF containing electrolytes has been demonstrated for model graphite electrodes, where the graphite was deposited on a disk [17]. In this work, an onset potential of around 2.0 V was reported for levels of HF of 60 ppm, and 2.5 V for 260 ppm. It should be noted, however, that these potentials cannot be directly compared to the potentials of the OEMS cell, due to the very different cell and electrode configurations. Similarly, in the study of Metzger *et al.* [44], a chemical source of protons was added to the electrolyte, methanesulfonic acid (MSA). Upon addition, hydrogen evolution, originating from a reduction process, started already at 2.3 V. In view of the very likely presence of HF in the electrolyte, originating from the reaction of PF_5 with water (eq. 1), the H_2 generation at 2.7 V in AR25 might be attributed to the reduction of HF according to

$$HF + Li^+ + e^- \rightarrow LiF + \tfrac{1}{2} H_2 \quad \text{(eq. 2)}$$

In fact, assuming that the initial water content of the electrolyte is around 20 ppm, an electrolyte volume of 500 µL corresponds to approximately 18 *n*mol of H_2O. The estimated release of POF_3 is around 7.5 *n*mol, which potentially leads to the formation of 15 *n*mol of HF if reaction (1) had been complete. The amount of hydrogen evolved in the course of the first peak is around 1.75 *n*mol, thus the proposed reaction mechanism seems plausible. Alternatively, it should also be noted that the THFIPB is also a likely source of protons, as the content of THFIPB (with 3 H per THFIPB) is significantly higher than the expected amount of HF originating from reactions with trace H_2O.

Once formed, there is also the risk that the presence of HF induces a series of autocatalytic reactions [11]. In the vicinity of the anode, within the SEI, the Li^+ solvation shell structure is disturbed and Li^+ may react with HF, thus generating LiF and a proton by the disproportionation reaction (eq. 3). Protons may then form ion pairs with PF_6^- and accelerate the anion decomposition according to eq. 3 and 4 [11].

$$Li^+ + HF \leftrightarrow LiF + H^+ \quad \text{(eq. 3)}$$

$$H^+ + PF_6^- \leftrightarrow HF + PF_5 \quad \text{(eq. 4)}$$

In Figure 4d, the C_2H_4 evolution onset potential is found at 1.1 V for both electrolytes, with a rapid upward and significantly higher evolution rate and a more positive peak potential in AR25. This can be rationalized in terms of EC reduction kinetics at the graphite/electrolyte interface, most commonly described by the equations 5 and 6, i.e., the main EC reduction products are assumed to be LEDC and C_2H_4, alternatively $LiCO_3$ and C_2H_4 [3, 45, 46]:

$$EC + 2e^- + 2Li^+ \rightarrow Li_2CO_3 + C_2H_4 \quad \text{(eq. 5)}$$

$$2EC + 2e- + 2Li+ \rightarrow (LiO_2COCH_2)_2 + C_2H_4 \quad \text{(eq. 6)}$$

It should be noted, however, that the 2 electron EC reduction mechanism suggested in eq. 5 is somewhat controversial, as Li_2CO_3 has frequently been suggested to be an artifact, resulting from reactions with CO_2 or moist [47]

The faster kinetics for the EC reduction in AR25 could be related to a more conductive and/or thinner SEI layer (less insulating solid products are formed). The result is in line with results obtained by Imhof and Novák [14], who found that the C_2H_4 evolution peak shifted to more negative values when water was added to the electrolyte, and also the Li^+ intercalation process appeared to be less reversible. Note that due to the extremely low scan rate applied for the OEMS measurements (25 μV/s), the current signal is noisy, in particular for the very low currents measured positive to the EC reduction potential, and therefore a quantitative comparison of the number of moles of gases formed in respect to the charge passed could be misleading.

There are three peaks of H_2 evolution for the LP30 electrolytes, with onset potentials of about 1.5, 1.0, and 0.2 V (Figure 4c), while for the AR25 electrolyte the peak around 1 V is not visible. The first one at 1.5 V is attributable to water reduction [13, 14]. The H_2 evolution rates in the LP30 electrolyte are higher than in the AR25 electrolyte, which could be

explained by the fact that residual water is already consumed by the accelerated hydrolysis reactions in AR25. The total amount of H_2 evolved is estimated to be around 23 *n*moles in both electrolytes, of which around 9.5 *n*moles are associated with the peaks recorded below 1.5 V for the AR25 electrolyte, whereas all H_2 evolution occurs below 1.5 V for the LP30 electrolyte. The origin of the peak separation into 3 distinct peaks is not clear. In our case, we observe that the second H_2 peak occurs just prior to the ethylene peak, and also we observe that the ethylene peak is sharper for the AR25 electrolyte, but at the same time the second H_2 peak is almost absent. We therefore propose that the second peak is also related to water reduction, but shifted relative to the first peak, due to changes in surface conditions related to the SEI forming reactions, as indicated in Ref. [14], and in line with the results for C_2H_4 emission (Figure 4d).

The last maximum of H_2 evolution occurs at about the same potential as the intercalation starts (0.2 V). Similarly, H_2 evolution was reported below 0.13 V, previously suggested to be related to the Li^+ intercalation into the graphite [48]. Therefore we interpret this as the reduction of the water strongly bound in the solvation shell of the Li^+ [14] accompanied by the charge transfer (Li^+ ion) at the graphite/SEI interface [14]. Alternatively, in Ref. [48], it is suggested that the intercalation process implies minor surface exfoliation, which enhances the H_2 evolution, most probably again due to reduction of residual water. The last H_2 peak is also shifted towards lower potential values in LP30 compared to AR25, in line with the differences in intercalation plateaus observed in Ref. [34].

CO_2 evolution is initiated at a potential of ca. 2.5 V in LP30. This high-potential CO_2 generation is absent when THFIPB is added. The source of this evolved CO_2 (Figure 4e), which is visible as two distinct peaks, and only for the LP30 electrolyte, is not known. A possible explanation is the reaction between the trace amounts of H_2O and some organic products formed on the surface. Species like $ROCO_2Li$ form spontaneously on the surface of metallic Li exposed to EC or DMC. The reaction between $ROCO_2Li$ with trace amounts of water will generate Li_2CO_3 and CO_2 [49]. In general, the reaction between organic EC reduction products and trace amounts of water will lead to the evolution of CO_2 whereas reaction with HF leads to the formation of LiF precipitates [50]. In addition, in a more recent study by Metzger *et* al [42], the H_2O driven hydrolysis of EC (not electrochemical) was suggested to result in evolution of CO_2 and formation of ethylene glycol, although with relatively high activation energy.

The CO_2 signal that peaks at about 1.25 V in both electrolytes is most likely due to the nucleophilic attack of the OH^- ions generated upon H_2O reduction at 1.5 V (eq. 7) on the EC molecules, as the positions of these peaks are overlapping. OH^- may then catalyze the EC ring opening [14] to yield CO_2 and di-alcoholates (eq. 8) [35, 51].

$$H_2O + e^- \rightarrow 1/2\ H_2 + OH^- \qquad \text{(eq. 7)}$$

$$OH^- + EC \rightarrow \text{di-alcoholates} + CO_2 \qquad \text{(eq. 8)}$$

For both electrolytes, the number of moles of CO_2 attributed to this main CO_2 peak is significantly higher than the number of moles of H_2 evolved in the same potential range (approximately 25 *n*mol for the LP30 electrolyte, 15 *n*mol for AR25). However, as shown in Ref [42], the OH-driven EC hydrolysis is autocatalytic. Provided that there is sufficient amount of water, as the formed di-alcoholate anion reacts with water to produce OH^-, which again decomposes the EC component. As the LP30 electrolyte has a higher content of water at this potential, and more OH^- is generated due to water reduction, it seems also reasonable that more CO_2 is generated in LP30, as is also observed in Figure 4e.

***XPS*--** XPS spectra were recorded for electrodes exposed to the respective electrolytes for 24 hrs, and cycled to 0.6 V, 0.21, and 0.17 V, as well as after 2 full cycles. The corresponding atomic % of the elements C, F, P, and O are shown in Table 1 for all these samples. The C1s, F1s, O1s, and P2p features of the graphite surface after exposure to the electrolytes LP30 and AR25 for 24 hrs are shown in Figure 6. The relative amount of Li is difficult to determine accurately due to its low cross section, and is therefore not reported.

The graphite electrode exposed to LP30 has features corresponding to what would be expected for a pristine electrode. The C1s features can be attributed to the carbon (C-C and C-H) as well as the binder phase (CH_2, CF_2 at around 286.5 and 290.5 eV, respectively). In addition, some electrolyte might be soaked in the binder phase, such that features from ethylene oxygen/ether (C-O) and carbonyl oxygen/carbonate (CO_3) (at 287 eV and 290.9 eV, respectively [52] [53]), may overlap with the binder features. The main peak of F1s may also be attributed to the binder, in addition there is a smaller peak corresponding to LiF (ca 1.5 atomic %), which indicate the presence of small amounts of electrolyte degradation products on the surface. Similarly, there is a small amount of phosphorous detected on the surface. LiF, P-F, and P-O features are normally attributed to salt decomposition products or salt residues. The main O1s feature (around 533 eV) is attributed to features from C-O bonds. In

addition, there is a small feature around 531 eV attributed to a carbonate, and also a feature at higher binding energies slightly above 534 eV. The origin of these could be either some trapped electrolyte (O1s spectra of carbonyl and ethylene bonds are found at 533 and 534.8 eV [52, 53]), electrolyte decomposition products and/or surface oxygen groups on the graphite or carbon black.

The sample stored in the AR25 electrolyte exhibit some differences in the surface chemistry, compared to the LP30 cycled electrode, as evident from Figure 4. The O1s feature around 533.5 eV (C-O) has grown, while the feature at 531 eV, normally associated with oxygen in carbonate, is small in comparison (the spectrum is asymmetric). The C1s peak at around 286 eV has also grown, and is larger than the peak around 290-291 eV, consistent with an increase in C-O linkages. The atomic % of C is significantly lower for AR25, indicating deposition of products on the surface (see Table 1). Also, there is a significant increase in the relative amounts of F and P, indicating electrolyte (salt) degradation products, including Li-F on the surface (see Table 1). The high-energy feature appearing in the C1s spectra (around 294 eV), originates most likely from CF_3 (i.e. THFIPB residue). Thus, as the P-F feature most likely overlaps with the C-F, some, but not all, of the fluorine originates from THFIPB. Trace amounts of THFIPB will also contribute to a growth of the C-O peak, but is unlikely the origin of all the oxygen.

In a previous study, where MCMB graphite powder was kept in 1M $LiPF_6$ in 1:1:1 EC:DMC:DEC for 4-10 days at 85 ^{o}C, similar results were found, i.e., a decrease of the relative atomic concentration of C was observed, as well as a small increase of F, P, and O [54]. The increase in oxygen was here associated with a shift in the O1s peak from 531 to 533 eV, and suggested to be related to a shift from carbonates to ethers, compatible with the presence of oligo and polyethylene oxides due to decarboxylation of the carbonates. This is consistent with the previously suggested catalytic effect of PF_5 on the ring-opening of EC [55]. Regarding the almost negligible O1s feature at 531 eV for the sample exposed to AR25, there is also the possibility that it is related to etching or conversion of some oxygen surface group. This would be consistent with the fact that, when assembled in half cells, the OCV of graphite electrodes against the lithium counter electrode is generally always > 3 V in LP30, while it is < 3 V (around 2.8 to 2.9 V) when assembled in AR containing electrolyte. Changes in the termination of edge carbon could be one possible explanation for this observation. The observed shifts in the peaks primarily attributed to binder/CH_2 and binder/CF_2 features, which however, contains contributions also from surface oxygen, supports this explanation

(the peaks are found at 286.9 and 290.9 eV vs. 286.3 and 290.3 eV for LP30 and AR25, respectively). The finding is also consistent with the lack of the CO_2 evolution at high potentials in AR, as observed by OEMS (Figure 4).

Figure 6 a–d shows the C1s, O1s, F1s, and P2p spectra of electrodes during the SEI forming process, i.e. electrodes were reduced to 0.6 V, 0.21 V, and 0.17 V in LP30 and AR25 electrolyte, respectively. These spectra were recorded with an excitation energy of 2005 eV. In addition, the 6015 eV spectra for C1s are shown in Figure 6 e (F1s and O1s spectra recorded at 6015 eV where very similar to the 2005 eV spectra). As expected, the C1s peaks associated with the C-C/C-H features are dominating at the highest potential (0.6 V). The SEI layer appears to be thinner in the AR25 samples, as may be inferred from the C-C/C-H features of both the 2005 and 6015 eV spectra (Figure 6a and e). There is more C and O in the surface of the LP30 sample at 0.6 V, attributed to organic compounds in the SEI, like LEDC, or the presence of di-alcoholates, consistent with the CO_2 peaks in the OEMS spectra (eqn. 8)

For both electrolytes, the C1s features at around 286.5 and 290.5 eV grow as the potential is lowered and SEI layer is formed. These features are associated with C-O bonds and carbonates, respectively, and overlap with the CH_2 and CF_2 features associated with the binder. The development of the C1s features are consistent with the O1s features, where peaks at around 531.5 and 533.5 eV are attributed to oxygen in carbonates, and C-O bonds, respectively. At 0.21 V, however, the oxygen content of the surface of the AR25 sample is higher, and dominated by the carbonate feature. While LEDC contribute to both the C-O and the carbonate feature, Li_2CO_3 is visible only in the carbonate feature at around 531.5 eV [5]. Thus, for AR25, significant amounts of Li_2CO_3 are detected in the SEI, and relatively low amounts of organic compounds at this potential (see Table 1).

For the lowest potential (0.17 V) as well as after two full cycles, the C1s and O1s spectra obtained at 2005 eV are relatively similar for the two electrolytes. It should be noted, however, that the results are dominated the outer parts of the SEI, known to be richer in organic components. The C-C feature is shifted to lower binding energies, as expected for lithiated graphite.

Regarding the F1s and P2p spectra (Figure 6d), in line with the results from the exposed, but not cycled samples (Figure 6), there are more salt reduction products, i.e. LiF, phosphate (P-O) and fluorophosphate (P-F) compounds in the AR25 samples at 0.6 V. For potentials lower

than 0.21 V, these features are similar in magnitude, with the exception of the phosphate features (P-O), which are significantly larger in the AR25 samples. At 0.6 V, the phosphate feature vanishes when using an excitation energy of 6015 eV (not included in figure), indicating that it is found mainly at the outer surface.

After two full cycles, the spectra for both electrolytes are very similar to those obtained after cycling to 0.17 V, an indication of formation of a stable SEI. For AR25, the C-C feature is smaller than both the C-O and carbonate features, indicating a thicker SEI layer of the AR25 sample compared to the LP30 sample. As may be inferred from the SEM micrographs, however, the SEI layer is more porous for AR25, which is also compatible with the presumably better conductivity [34]. For the spectra recorded at 6015 eV, small differences were observed in the C1s spectra, but not in the others. The C1s spectra are therefore included in Figure 6e, and show primarily that the C-C feature is lower compared to the others for the AR25 sample after 2 full cycles, indicating a thicker SEI. For the LP30 sample, the fraction of organic SEI compounds is lower at the higher excitation energy, corresponding to the inner parts of the SEI.

DRIFT analysis of charged electrodes--- The graphite electrodes were galvanostatically charged at 10 mA/g rate from OCP to 1.4 V, 0.9 V, and 10 mV in LP30 and AR25, where a potentiostatic step was included until the current dropped to 10% of the initial value. DRIFT spectra of the cycled electrodes are shown in Figure 7a. There is a gradual increment in peak intensities as the electrodes are cycled to lower potentials. After cycling to 10 mV (*vs.* Li/Li^+), spectral features in both electrolytes around 1410 cm^{-1} are attributed to Li_2CO_3 in accordance with previous works [56, 57, 58] and the reference spectrum (Figure 7b). Peaks around 1660 cm^{-1} [59, 60, 61], 1460 cm^{-1}, 1320 cm^{-1} [59, 61], and 830 cm^{-1} [59, 60, 61] in both electrolytes are consistent with previous reports and assigned to C=O asymmetric stretching, CH_2 bending, CH_2, C=O symmetric stretching, and out of plane bending of CO_3 in LEDC species, respectively. The absorptions around 1770-1800 cm^{-1} are most likely due to C=O stretching and, based on previous works [57, 61, 62] as well as the FTIR spectra of EC (Figure 7b), it may be assigned to EC residue which is difficult to remove even after washing the electrodes owing to its low melting temperature [61]. The absorption around 1190-1200 cm^{-1} is typically diagnostic for C-F bond arising from the PVDF binder in the electrode paste [59, 61, 62]. The band around 850 cm^{-1} may be attributed to P-F vibrations [57]. Comparison of the two spectra reveals that both Li_2CO_3/LEDC and P-F/LEDC ratios are higher in AR25 at 10 mV, Figure 7c).

Operando XRD studies of graphite electrodes--- In-situ XRD patterns of the graphite were recorded during the first charge at 10 A/kg in LP30 and AR25. The X-ray scans at 250 mV and 202 mV are shown in Figure 8 to verify the shift in Li^+ intercalation potential between LP30 and AR25 electrolytes. At 250 mV there is no intercalation in neither of the electrolytes, and the X-ray spectra of the graphite electrodes shows identical peaks at ~26.2 degrees for both electrolytes (Figure 8b), corresponding to the (002) reflections of graphite. When the potential decreases to 202 mV, the intercalation has already made progress in AR25, whereas there is no intercalation in LP30 (Figure 8a). The coexistence of two peaks for AR25 indicates that the transformation to the lower stage has not been completed and the intercalation is still ongoing at this potential. The X-ray scan of graphite at 202 mV in LP30, however, shows that the (002) peak of graphite is retained at 26.2 (Figure 8c). As demonstrated in our previous work [34], the intercalation potential is slightly positive in the first cycle for the AR25 electrolyte compared to LP30 (but not in subsequent cycles). As the current during the experiment is very low (10 mA/g), we consider it unlikely that the shift in the potential is related to differences in the resistance of the electrolyte, the already formed SEI, or the Li counter electrode. The most likely explanation for the observed difference in degree of lithiation is the fact the initial SEI forming reactions are also different, with corresponding differences in kinetics (as observed from OEMS and XPS results). This will affect the share of current for SEI formation and lithiation during a galvanostatic experiment at low rate, as SEI formation is still ongoing at potentials around 200 mV.

In Ref. [63] it was demonstrated how differences in local overpotentials for the SEI forming reactions would help suppress unwanted side-reactions (in this case exfoliation). Also, it is possible that eventually the thermodynamic potential of intercalation is shifted due to solvation effects, as shown for sodium intercalation in graphite earlier [64]. However, as the shift in the intercalation potential is observed in the first cycle only [34], we consider the first explanation the most likely, and also in good agreement with the OEMS and XPS results obtained.

To summarize briefly the results presented, the formation of primarily organic SEI compounds in LP30 electrolyte, starting already from high potentials and related to the presence of water, helps to passivate the surface. This is directly seen from the C1s and O1s features in the XPS spectra, clearly indicating the presence of organic species at 0.6 V for the LP30 electrolyte, and indirectly from the OEMS measurements, where the early onset of the CO_2 evolution for LP30 is compatible with for example products formed during reactions

with trace amounts of H_2O, or H_2O driven hydrolysis of EC. At high potentials, primarily salt reduction products were observed for the AR25 electrolyte, and also significantly more LiF, and P-F features are observed after exposure of electrodes to this electrolyte compared to the LP30 electrolyte. At 0.6 V, there are still few organic products on the surface for the AR25 electrode, and the kinetics of the EC reduction is improved, as seen by the C_2H_4 evolution from the OEMS cell, which exhibit a sharp peak with a higher onset potential than the C_2H_4 peak from the LP30 cell. After 2 full cycles, the SEI layers are relatively similar, only slightly thicker for the AR25 electrolyte. From the previous study of the electrochemical performance, the LP30 electrolyte resulted in a more resistive but certainly better passivating SEI, as observed by the higher coulombic efficiency [34]. SEM micrographs of cycled electrodes showed that the anode cycled in LP30 displayed a continuous SEI that even extending between the graphite particles. Some graphite particles were seen to be isolated, which could possibly be the reason for the inferior cycling stability. In contrast, the AR25 cell showed a completely different SEI layer, dominated by two layers of granular morphology. Here, we show that that for AR25 formation of the SEI involves to a larger extent the deposition of salt reduction products which happens already at high potentials, or even by exposure to the electrolyte. In comparison to LP30, the SEI is enriched in inorganic compounds, with a high fraction of Li_2CO_3, as confirmed by both XPS and DRIFT measurements. From a more practical viewpoint, the results illustrate the importance of good temperature control during assembling and initial formation of Li-ion cells.

Conclusions

THFIPB addition to a commercial LP30 electrolyte alters the electrolyte structure and thus changes the SEI formation on a graphite anode. The THFIPB accelerates anion decomposition by capturing F^- from the salt anion, and thus more electrolyte decomposition products are found in the THFIPB containing electrolyte, like HF, PF_5, and POF_3.

During the initial SEI formation in the THFIPB containing electrolyte, some of the HF species formed probably react further to evolve H_2 gas at rather high potentials, thus the amount of residual water is lower. The water may react with products formed at higher potentials, or hydrolyze EC, which is in line with the onset of CO_2 evolution at higher potentials in LP30, likely having less HF and more water. Water is reduced at lower potentials, and H_2 gas evolves, associated with formation of OH^-, which again may accelerate decomposition of EC. During the early stages of the SEI formation, the surface of the LP30

samples appears to be more covered with organic products, and also more H_2 evolves from water reduction.

EC reduction is facilitated by THFIPB addition as shown by a sharp C_2H_4 evolution peak located at more positive potential than that in LP30. There is less gaseous CO_2 and H_2 formed during the initial formation cycle in the presence of THFIPB. The SEI formed in the electrolyte with added THFIPB is richer in inorganic compounds, both salt reduction products as well as Li_2CO_3, as compared to the LP30 electrolyte, which has relatively more organic SEI compounds, also at potentials around 1 V. This results in a chemically modified SEI, which also exhibits improved intercalation kinetics in the first cycle.

Acknowledgments

This work was funded by the Norwegian University of Science and Technology. The Paul Scherrer Institute in Switzerland is acknowledged for supporting the experimental work.

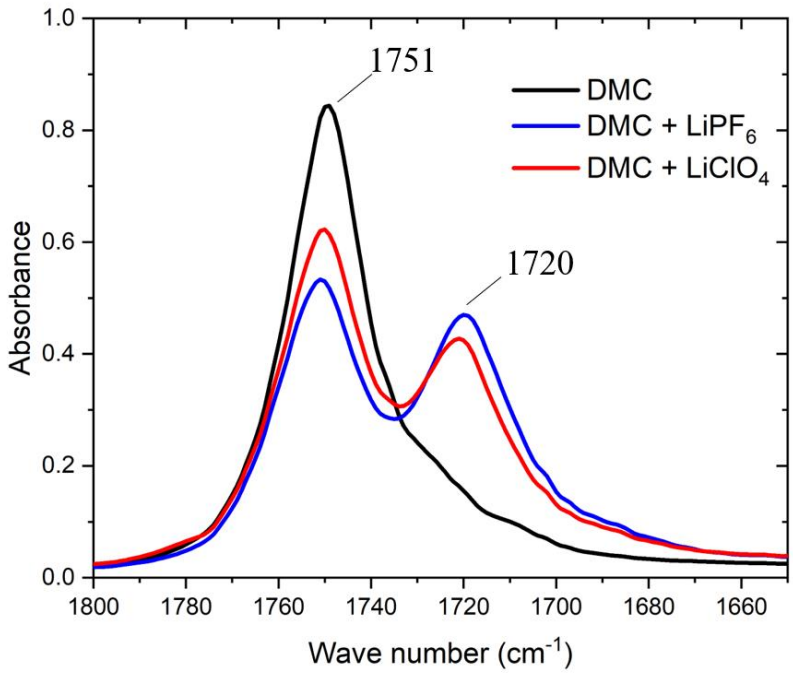

Figure 1. FTIR spectra (absorbance mode) of various electrolyte components including $LiPF_6$, $LiClO_4$, DMC and their mixtures. Absorptions of interest for discussion are highlighted on the absorption peaks.

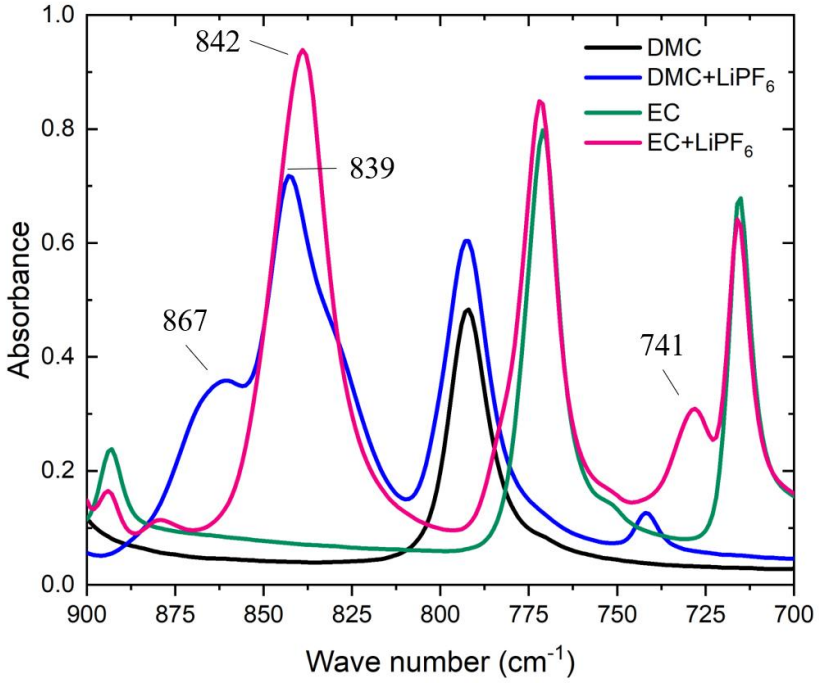

Figure 2. FTIR spectra (absorbance mode) of various electrolyte components including DMC, EC and their mixtures with $LiPF_6$. Absorptions of interest for discussion are highlighted on the absorption peaks.

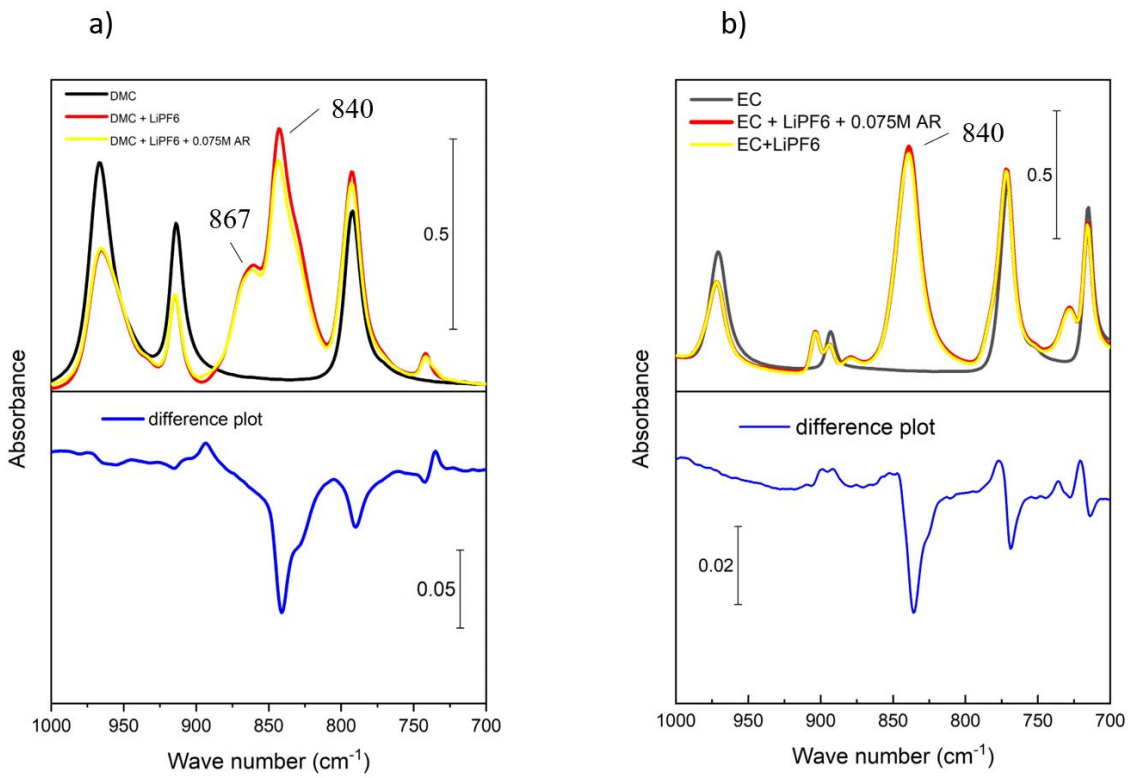

Figure 3. FTIR analysis of the solvent/salt/THFIPB mixtures **a)** FTIR spectrum of DMC, DMC+1M $LiPF_6$, and DMC+1M $LiPF_6$+0.075M THFIPB, together with the difference spectrum of DMC+1M $LiPF_6$, and DMC+1M $LiPF_6$+0.075M THFIPB. **b)** FTIR spectrum of EC, EC+1M $LiPF_6$, and EC+1M$LiPF_6$+0.075M THFIPB, together with the difference spectrum of EC+1M $LiPF_6$, and EC+1M $LiPF_6$+0.075M THFIPB.

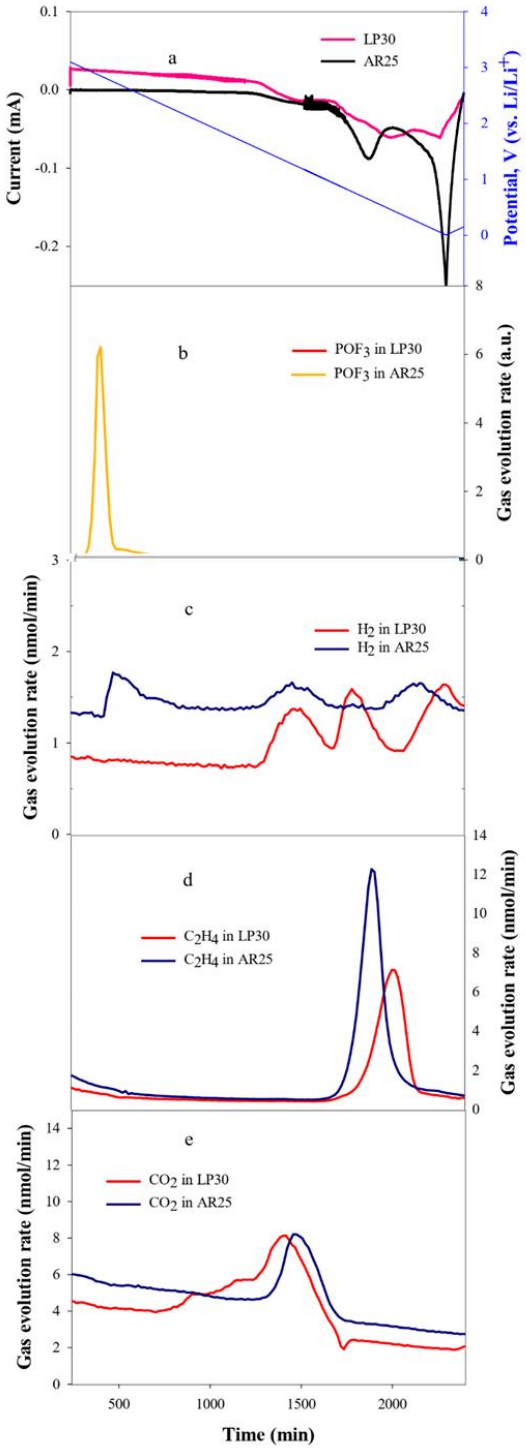

Figure 4. **a)** Linear sweep voltammograms of Li/SLP30 OEMS half cells with LP30 and AR25, **b-e)** reaction gases evolving from the cells during negative potential sweep for the first time in LP30 and AR25 electrolytes. Sweep rate: 25 µV/s; Cut-off potential: 5 mV (vs. Li/Li^+).

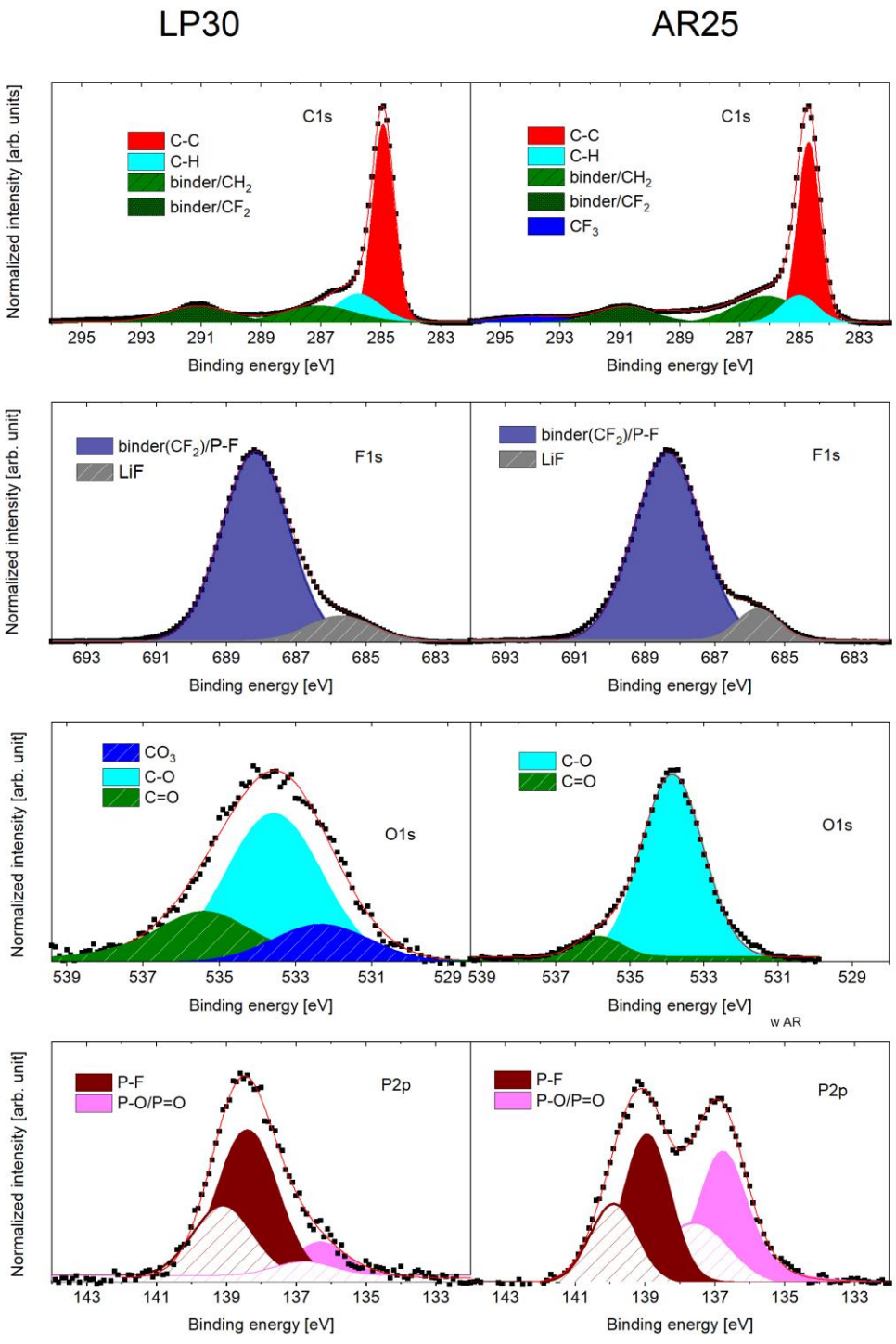

Figure 5. C1s, F1s, O1s and P2p HAXPES spectra of graphite electrodes exposed to LP30 and AR25 for 24 hrs. Excitation energy of 2005 eV.

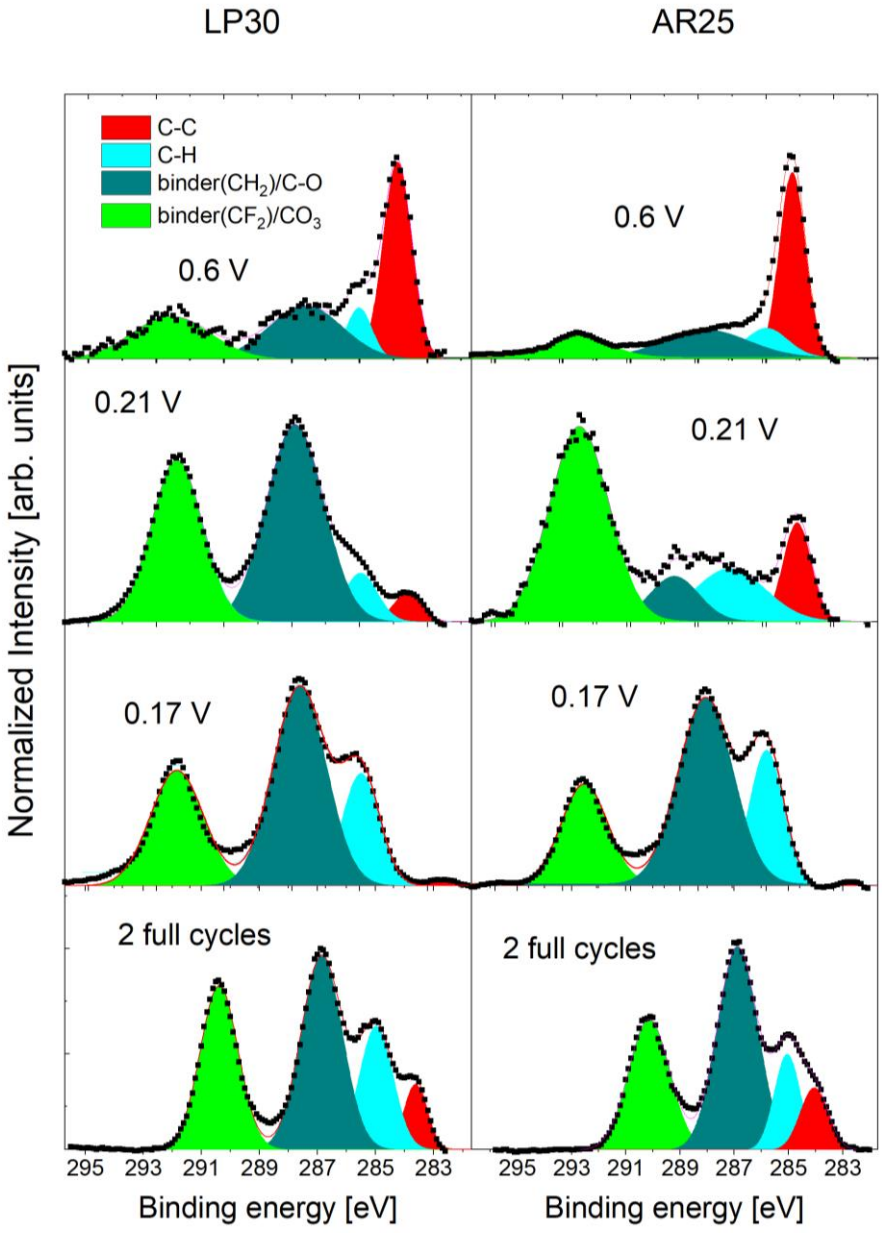

Figure 6 a) C1s HAXPES spectra of graphite electrodes stopped at different potentials during the first two cycles in LP30 and AR25 electrolytes. Excitation energy of 2005 eV

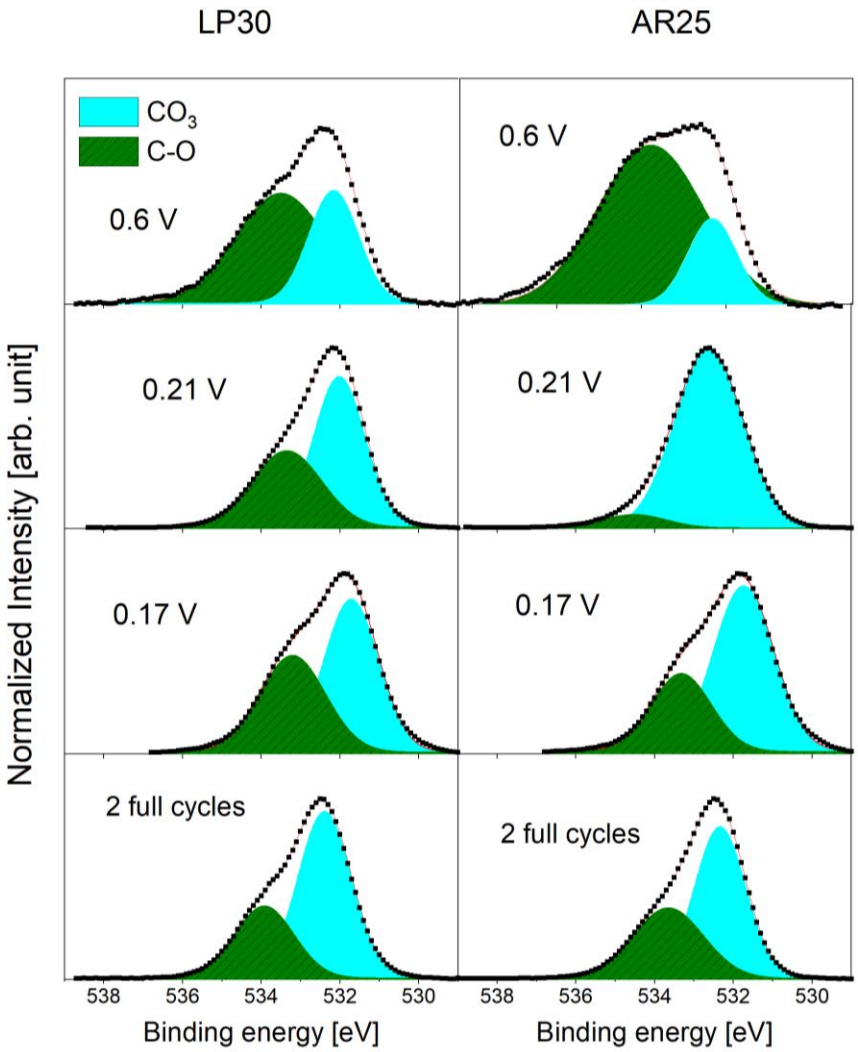

Figure 6 b) O1s HAXPES spectra of graphite electrodes stopped at different potentials during the first two cycles in LP30 and AR25 electrolytes. Excitation energy of 2005 eV

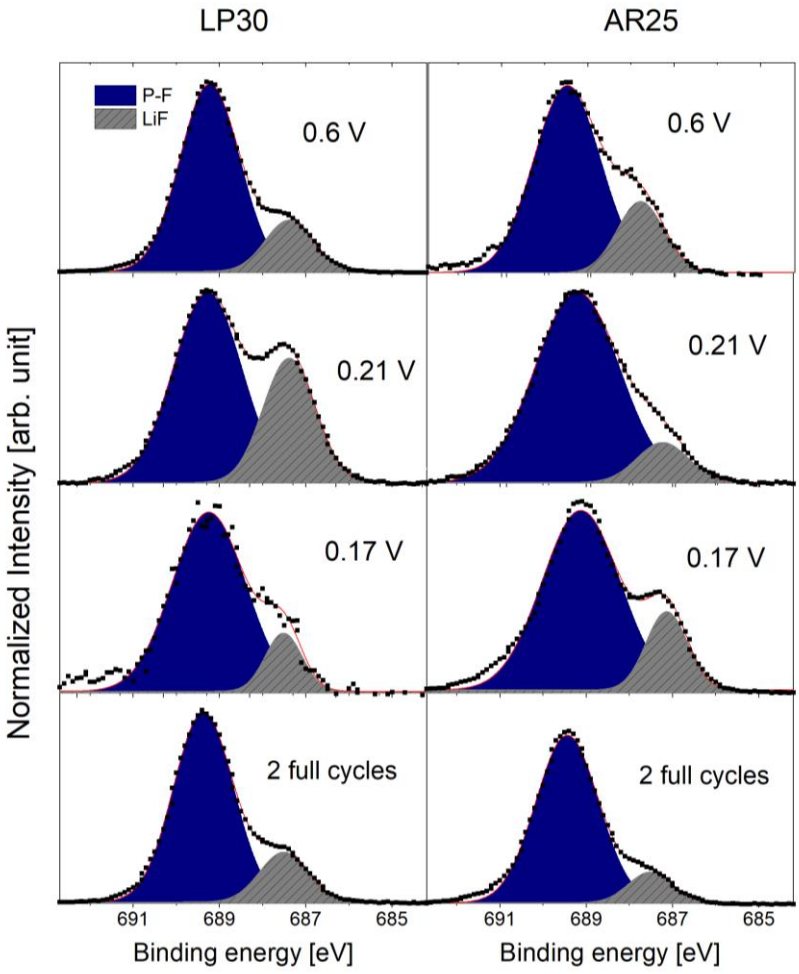

Figure 6 c) F1s HAXPES spectra of graphite electrodes stopped at different potentials during the first two cycles in LP30 and AR25 electrolytes. Excitation energy of 2005 eV

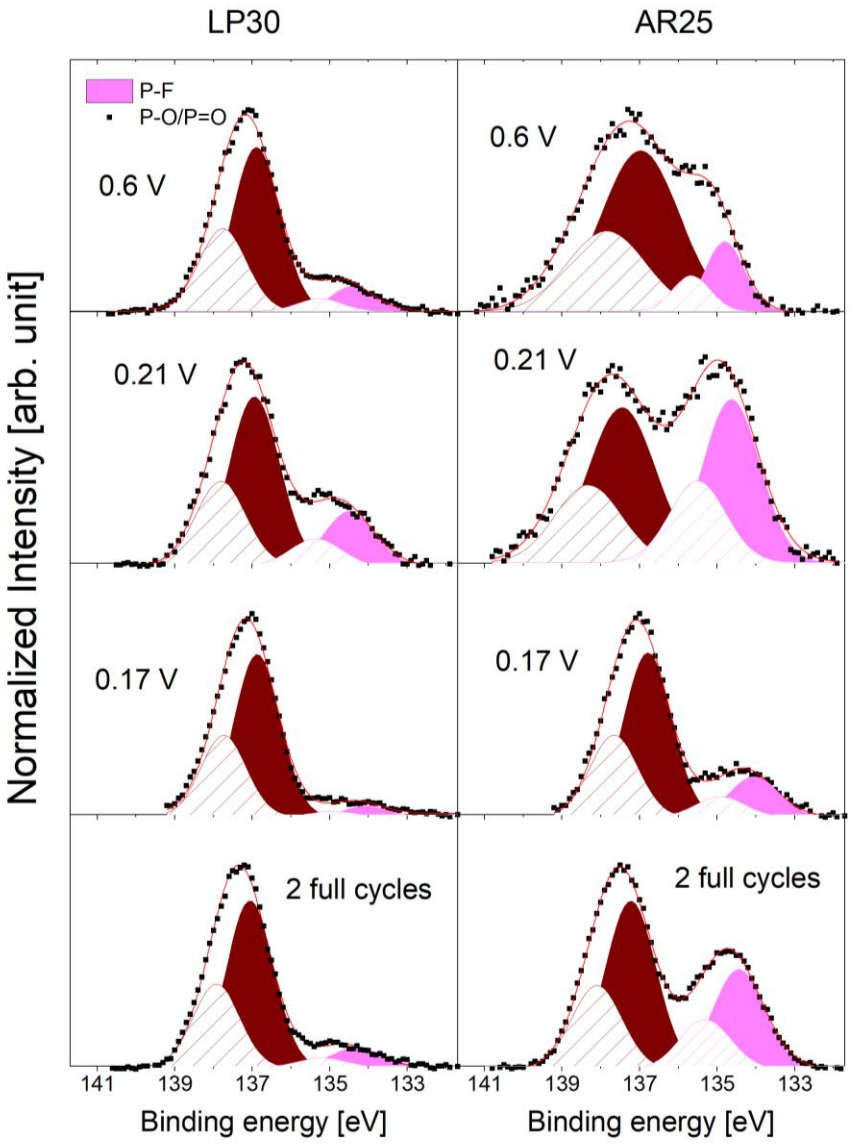

Figure 6 d) P2p HAXPES spectra of graphite electrodes stopped at different potentials during the first two cycles in LP30 and AR25 electrolytes. Excitation energy of 2005 eV

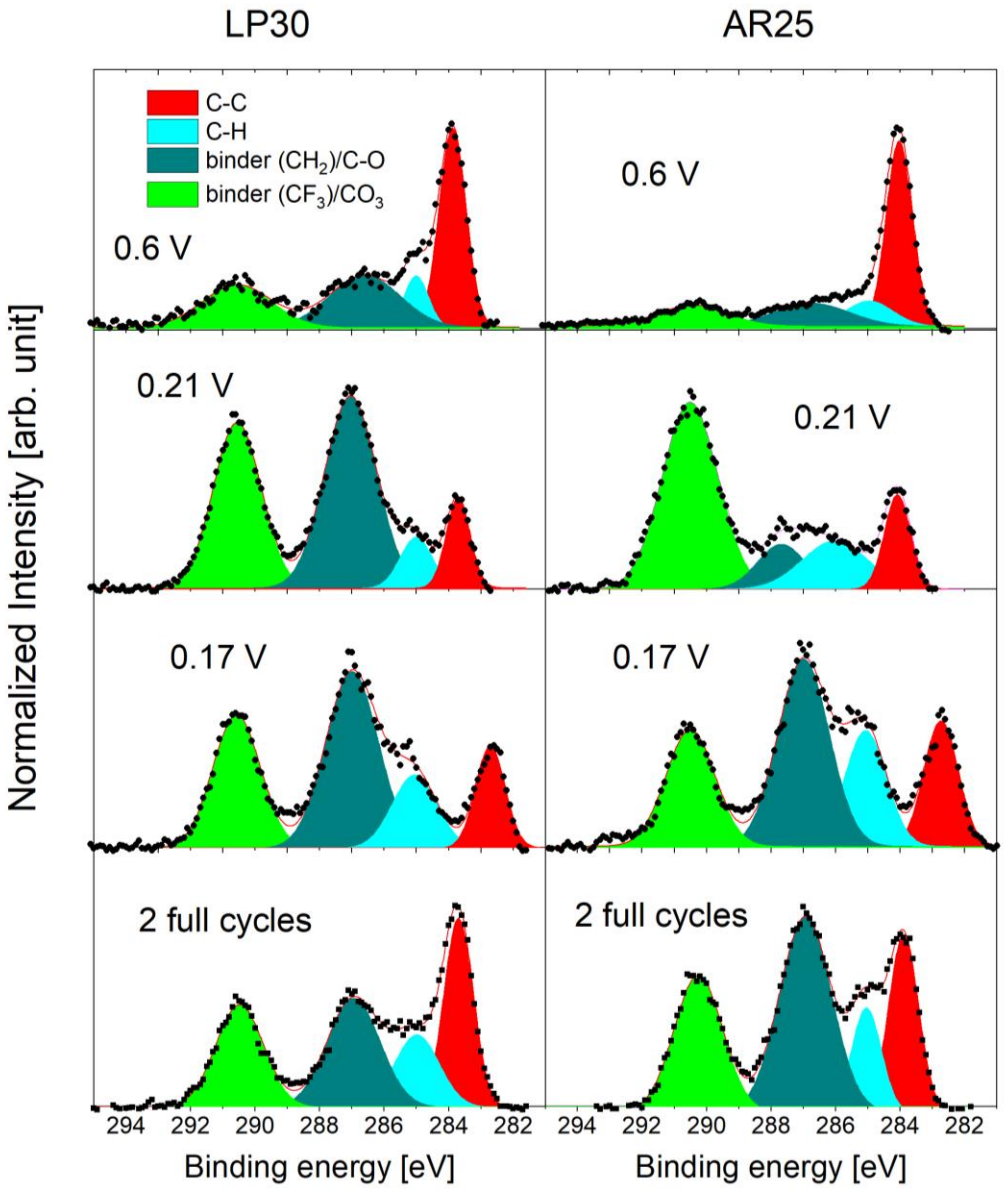

Figure 6 e) C1s HAXPES spectra of graphite electrodes stopped at different potentials during the first two cycles in LP30 and AR25 electrolytes. Excitation energy of 6015 eV

a)

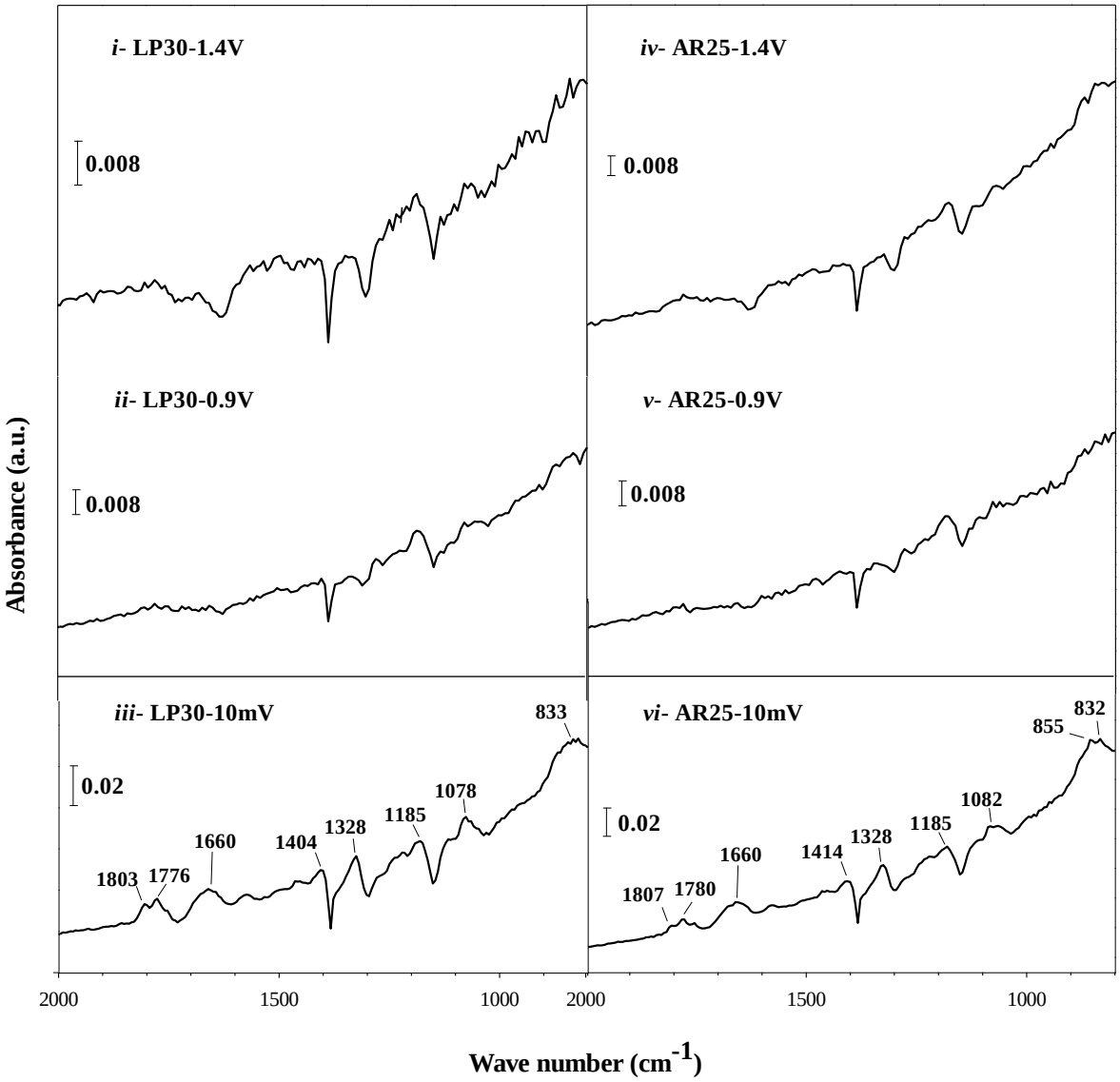
i- LP30-1.4V
0.008
iv- AR25-1.4V
0.008
ii- LP30-0.9V
0.008
v- AR25-0.9V
0.008
iii- LP30-10mV
0.02
833
1078
1185
1328
1404
1660
1776
1803
vi- AR25-10mV
0.02
832
855
1082
1185
1328
1414
1660
1780
1807
Absorbance (a.u.)
2000
1500
1000
2000
1500
1000
Wave number (cm-1)

b) c)

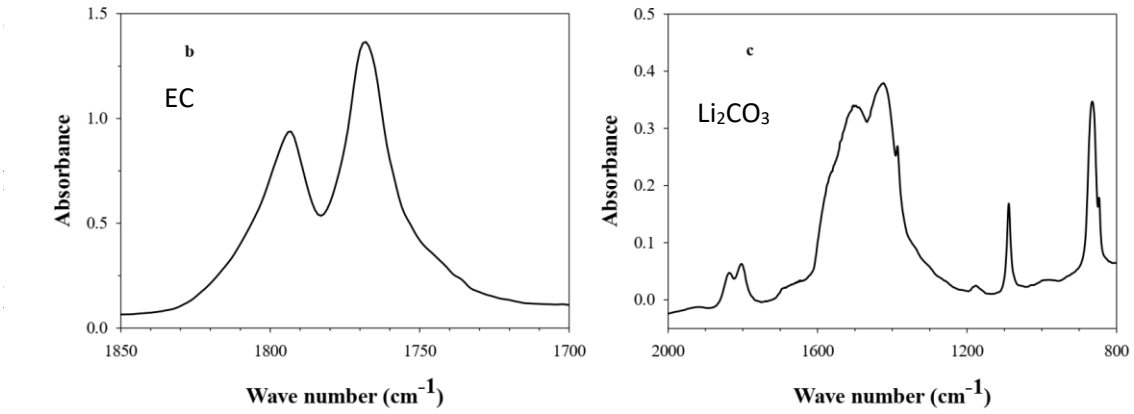

d)

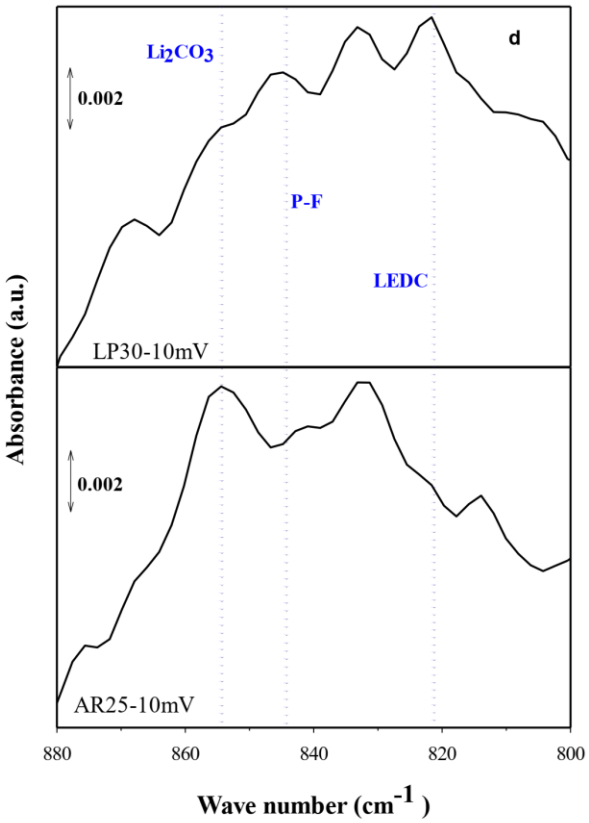

Figure 7. DRIFT spectra of graphite electrodes **a)** after discharged to *i*) 1.4V, *ii*) 0.9V, *iii*) 10mV in LP30, and *iv*) 1.4V, *v*) 0.9V, *vi*) 10mV in AR25, **b)** FTIR spectrum of EC **c)** DRIFT plot of Li_2CO_3, **d)** DRIFT plot of graphite electrodes charged to 10 mV.

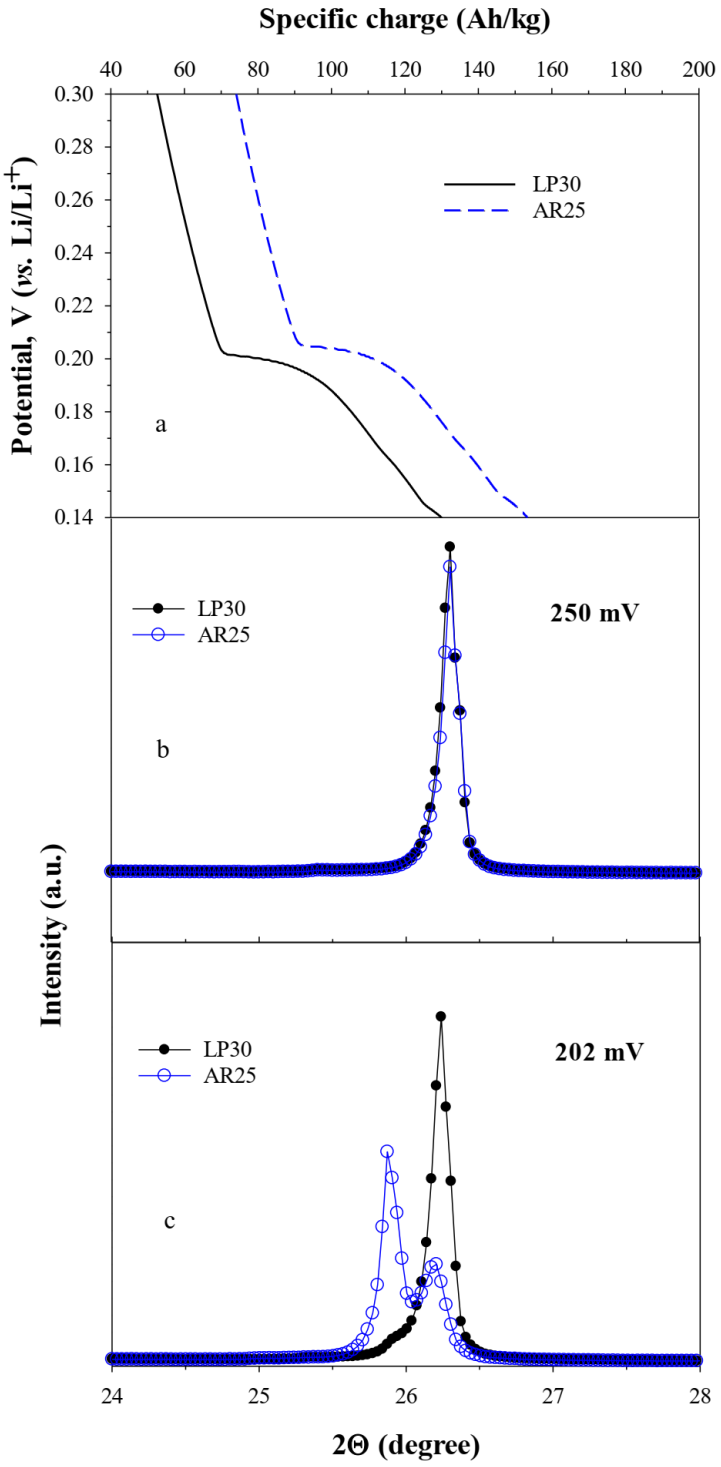

Figure 8. a) Potential profiles of graphite electrodes for the first charging in LP30 and AR25. Corresponding operando X-ray diffractograms recorded during the charging, **b)** at 250 mV and **c)** at 202 mV.

TABLES

Table 1. Atomic % evaluated from the XPS spectra of the surface of graphite electrode after exposure to LP30 or AR25 electrolyte for 24 hrs.

Element\Potential	OCV LP30	OCV AR	0,6 V LP30	0,6 V AR	0,21 V LP30	0,21 V AR	0,17 V LP30	0,17 V AR	2 full, LP30	2 full, AR
C1s	**78.4**	**60.5**	**52.6**	**55.6**	**37.4**	**29.1**	**38.1**	**42.2**	**42.4**	**34.3**
C-C	43.8	29.5	20.8	27.4	1.4	3.9	0.9	1.3	3.2	3.3
C-H	12.8	11.8	4.8	7.1	2.8	5.4	7.4	9.6	8.8	4.7
C-O/CH_2(binder)	11.5	10.6	14.5	13.3	19.2	3.2	18.9	21.5	17.1	15.9
CO_3/CF_2(binder)	10.3	6.0	12.4	7.8	14.0	16.6	10.9	9.8	13.3	10.3
CF_3		2.6								
O1s	**8.0**	**12.3**	**20.2**	**12.1**	**47.5**	**59.3**	**36.0**	**35.8**	**35.3**	**40.6**
CO_3	1.2		7.3	2.4	28.3	55.3	20.4	24.3	23.8	24.8
C-O	4.6	11.4	12.9	9.7	19.2	4.0	15.5	11.5	11.4	15.8
C=O	2.2	0.9	-	-	-	-	-	-	-	-
F1s	**13.0**	**24.9**	**25.8**	**30.3**	**14.2**	**10.4**	**23.9**	**20.5**	**20.8**	**21.8**
LiF	1.5	2.3	4.6	6.4	4.7	1.2	3.3	3.9	3.7	2.4
P-F/binder	11.5	22.6	21.1	23.9	9.5	9.2	20.6	16.6	17.1	19.4
P2P	**0.5**	**2.1**	**1.6**	**1.9**	**1.0**	**1.6**	**2.1**	**1.5**	**1.5**	**3.3**
P-O	0.1	1.2	0.2	0.3	0.2	0.8	0.1	0.3	0.2	1.3
P-F	0.4	0.9	1.4	1.6	0.7	0.8	1.9	1.2	1.3	2.1

REFERENCES

[1] D. Aurbach, Nonaqueous Electrochemistry, NY: Marcel Dekker, 1999.

[2] P. Verma, P. Maire and P. Novák, *Electrochim. Acta,* vol. 55, pp. 6332-6341, 2010.

[3] M. Nie, D. Chalasani, D. Abraham, Y. Chen, A. Bose and B. Lucht, *J. Phys. Chem. C,* vol. 117, pp. 1257-1267, 2013.

[4] C. Lee, J. Dura, A. LeBar og S. DeCaluwe, *J. Power Sources,* vol. 412, pp. 725-735, 2019.

[5] K. Høgstrøm, S. Malmgren, M. Hahlin, M. Gorgoi, L. Nyholm, H. Rensmo og K. Edstrøm, *Electrochim. Acta,* vol. 138, pp. 430-436, 2014.

[6] N. Takenaka, Y. Suzuki, H. Sakai og M. Nagaoka, *J. Phys. Chem. C,* vol. 118, nr. 20, pp. 10874-10882, 2014.

[7] K. Edström, M. Herstedt and D. Abraham, *J. Power Sources,* vol. 153, pp. 380-384, 2006.

[8] J. Pan, Q. Zhang, X. Xiao, Y. Cheng og Y. Qi, *ACS Appl. Mater. Interfaces,* vol. 8, pp. 5687-5693, 2016.

[9] Q.L. Zhang, J. Pan, P. Lu, Z. Liu, M. Verbrugge, B. Sheldon, Y. Cheng, Y. Qi og X. Xiao, *Nano Letters,* vol. 16, pp. 2011-2016, 2016.

[10] S. Lux, I. Lucas, E. Pollak, S. Passerini, M. Winter and R. Kostecki, *Electrochem. Comm.,* vol. 14, pp. 47-50, 2012.

[11] A. Plakhotnyk, L. Ernst and R. Schmutzler, *J. Fluorine Chem.,* vol. 126, pp. 27-31, 2005.

[12] M. Moshkovich, Y. Gover og D. Aurbach, *J. Electrochem. Soc. ,* vol. 148, pp. E155-E167, 2001.

[13] R. Bernhard, M. Metzger and H. Gasteiger, *J. Electrochem. Soc.,* vol. 162, no. 10, pp. A1984-A1989, 2015.

[14] R. Imhof and P. Novak, *J. Electrochem. Soc.,* vol. 145, no. 4, pp. 1081-1087, 1998.

[15] D. Aurbach og H. Gotlieb, *Electrochim. Acta,* vol. 34, p. 141, 1989.

[16] S. Sloop, J. Kerr and K. Kinoshita, *J. Power Sources,* Vols. 119-121, pp. 330-337, 2003.

[17] D. Strmcnik, I. Castelli, J. Connell, D. Haering, M. Zorko, P. Martins, P. Lopes, B. Genorio, T. Østergaard, H. Gasteiger, F. Maglia, B. Antonopoulos, V. Stamenkovic, J. Rossmeisl og N. Markovic, *Nature catalysis,* vol. 1, pp. 255-262, 2018.

[18] R. McMillan, H. Slegr, Z. X. Shu og W. Wang, *J. Power Sources,* Vol. %1 av %281-82, pp. 20-26, 1999.

[19] R. Mogi, M. Inaba, S.-K. Jeong, Y. Iriyama, T. Abe og Z. Ogumi, *J. Electrochem. Soc.,* vol. 149, pp. A1578-A1583, 2002.

[20] N.-S. Choi, K. H. Yew, K. Y. Lee, M. Sung, H. Kim og S.-S. Kim, *J. Power Sources,* vol. 161, pp. 1254-1259, 2006.

[21] L. Ma, S. L. Glazier, R. Petibon, J. Xia, J. M. Peters, Q. Liu, J. Allen, R. N. C. Doig og J. R. Dahn, *J. Electrochem. Soc.,* vol. 164, p. A5008−A5018, 2017.

[22] D. Aurbach, K. Gamolsky, B. Markovsky, Y. Gofer, M. Schmidt and U. Heider, *Electrochim. Acta,* vol. 47, pp. 1423-1439, 2002.

[23] M. Contestabile, M. Morselli, R. Paraventi and R. Neat, *J. Power Sources,* Vols. 119-121, pp. 943-947, 2003.

[24] T. Sasaki, T. Abe, Y. Iriyama, M. Inaba and Z. Ogumi, *J. Electrochem. Soc.,* vol. 152, no. 10, pp. A2046-A2050, 2005.

[25] H. Lee, X. Yang and J. McBreen, *J. Electrochem. Soc.,* vol. 145, no. 8, pp. 2813-2818, 1998.

[26] X. Sun, H. Lee, X. Yang and J. McBreen, *J. Electrochem. Soc.,* vol. 146, no. 10, pp. 3655-3659, 1999.

[27] Z. Chen and K. Amine, *J. Electrochem. Soc.,* vol. 153, no. 6, pp. A1221-A1225, 2006.

[28] M. Herstedt, M. Stjerndahl, T. Gustafsson and K. Edström, *Electrochem. Commun.,* vol. 5, pp. 467-472, 2003.

[29] Z. Chen and K. Amine, *Electrochem. Commun,* vol. 9, pp. 703-707, 2007.

[30] Y. Qin, Z. Chen, H. Lee, X. Yang and K. Amine, *J. Phys. Chem. C,* vol. 114, pp. 15202-15206, 2010.

[31] S. Zhang, K. Xu og T. Jow, *Electrochemical and Solid State Letters,* vol. 5(9), pp. A206-A208, 2002.

[32] W. West, J. Whitacre, N. Leifer, S. Greenbaum, M. Smart, B. Ratnakumar, M. Blanco and S. Narayanan, *J. Electrochem. Soc.,* vol. 154, no. 10, pp. A929-A936, 2007.

[33] Z. Chen and K. Amine, "Computational Estimates of Fluoride Affinity of Boron-Based Anion Receptors," *J. Electrochem. Soc. ,* vol. 156, no. 8, pp. A672-A676, 2009.

[34] A. Tezel, S. Sunde, J. Gomez-Camer, P. Novak and A. Svensson, *J. Electrochem. Soc. ,* vol. 167, p. 20525, 2020.

[35] M. He, E. Castel, A. Laumann, G. Nuspl, P. Novák and E. Berg, *J. Electrochem. Soc.,* vol. 162, no. 6, pp. A870-A876, 2015.

[36] A. Andersson and K. Edstrom, *J. Electrochem. Soc.,* vol. 148, no. 10, pp. A1100-A1109, 2001.

[37] R. Aroca, M. Nazri, G. Nazri, A. Camargo and M. Trsic, *J. Solution. Chem.,* vol. 29, no. 10, pp. 1047-1060, 2000.

[38] M. Burba and R. Frech, *J. Phys. Chem. B,* vol. 109, pp. 15161-15164, 2005.

[39] A. Cresce, M. Gobet, O. Borodin, J. Peng, S. Russell, E. Wikner, A. Fu, L. Hu, H. Lee, Z. Zhang, X. Yang, S. Greenbaum, K. Amine and K. Xu, *J. Phys. Chem. C,* vol. 119, pp. 27255-27264, 2015.

[40] J. Katon og M. Cohen, *Can. J. Chem.,* vol. 53, pp. 1378-1386, 1975.

[41] C. Bolli, A. Gueguen, A. Mendez og E. Berg, *Chemistry of Materials,* vol. 31, pp. 1258-1267, 2019.

[42] M. Metzger, B. Strehle, S. Solchenbach and H. Gasteiger, *J. Electrochem. Soc.,* vol. 163, no. 7, pp. A1219-A1225, 2016.

[43] F. Joho, B. Rykart, R. Imhof, P. Novak, M. Spahr and A. Monnier, *J. Power Sources,* Vols. 81-82, pp. 243-247, 1999.

[44] M. Metzger, S. Strehle, S. Solchenbach and H. Gasteiger, *J. Electrochem. Soc.,* vol. 163, no. 5, pp. A798-A809, 2016.

[45] D. Aurbach, E. Zinigrad, Y. Cohen og H. Teller, *Solid State Ionics ,* vol. 148, p. 405, 2002.

[46] S. Leroy, F. Blanchard, R. Dedryvere, H. Martinez, B. Carre, D. Lemordant og D. Gonbeau, *Surf. Interface Anal.,* vol. 37, p. 773, 2005.

[47] K. Xu, *Chem. Rev. ,* vol. 114, pp. 11503-11618, 2014.

[48] F. Mantia and P. Novak, *Electrochem. Solid-State Lett.,* vol. 11, no. 5, pp. A84-A87, 2008.

[49] D. Aurbach, Y. Ein-Ely and A. Zaban, *J. Electrochem. Soc,* vol. 141, no. 1, pp. L1-L3, 1994.

[50] D. Aurbach, A. Zaban, E. Ein-Eli, I. Weissman, O. Chusid, B. Markovsky, M. Lvi, E. Levi, A. Schechter and M. Granolt, *J. Power Sources,* vol. 68, pp. 91-98, 1997.

[51] R. Bernhard, S. Meini and H. Gasteiger, *J. Electrochem. Soc.,* vol. 161, no. 4, pp. A497-A505, 2014.

[52] R. Dedryvere, L. Gireaud, S. Grugeaon, S. Laruelle og J. Tarascon, *J. Phys. Chem. B,* vol. 109, pp. 15868-15875, 2005.

[53] M. Fingerle, T. Spath, N. Schulz and R. Hausbrand, *Chemical Physics,* Vols. 498-499, pp. 19-24, 2017.

[54] A. Xiao, W. Li og B. Lucht, *J. Power Sources,* vol. 162, p. 128, 2006.

[55] S. Sloop, J. K. Pugh, S. Wang, J.B. Kerr og K. Kinoshita, *Electrochem. and Solid State Letters,* vol.

4, p. A42, 2001.

[56] M. Brooker and J. Bates, *J. Chem. Phys.,* vol. 54, pp. 4788-4796, 1971.

[57] D. Aurbach, A. Zaban, A. Schechter, Y. Ein-Eli, E. Zinigrad and B. Markovsky, *J. Electrochem. Soc.,* vol. 142, no. 9, pp. 2873-2882, 1995.

[58] L. Li, B. Xie, H. Lee, H. Li, X. Yang, J. McBreen and X. Huang, *J. Power Sources,* vol. 189, pp. 539-542, 2009.

[59] D. Aurbach, M. Levi, E. Levi and A. Schechter, *J. Phys. Chem. B,* vol. 101, pp. 2195-2206, 1997.

[60] M. Nie, D. Chalasani, D. Abraham, Y. Chen, A. Bose and B. Lucht, *J. Phys. Chem. C,* vol. 117, pp. 1257-1267, 2013.

[61] D. Aurbach, B. Markovsky, A. Shechter and Y. Ein-Eli, *J. Electrochem. Soc.,* vol. 143, no. 12, pp. 3809-3820, 1996.

[62] D. Aurbach, Y. Ein-Eli and O. Chusit, *J. Electrochem. Soc.,* vol. 141, no. 3, pp. 603-611, 1994.

[63] D. Goers, M. Spahr, A. Leone, W. Markle og P. Novak, *Electrochimica Acta,* vol. 56, pp. 3799-3808, 2011.

[64] M. Göktas, C. Bolli, E. Berg, P. Novák, K. Pollok, F. Langenhorst, M. Roeder, D. Lenchuk, D. Mollenhauer og P. Adelhelm, *Adv. Energy Materials,* vol. 8, p. 1702724, 2018.